Inorganic Chemistry

ARTICLE

pubs.acs.org/IC

Shape-Controlled Synthesis of Well-Defined Matlockite LnOCl (Ln: La, Ce, Gd, Dy) Nanocrystals by a Novel Non-Hydrolytic Approach

Kenneth R. Kort and Sarbajit Banerjee*

Department of Chemistry, University at Buffalo, State University of New York, Buffalo, New York 14260-3000, United States

Supporting Information

ABSTRACT: We report here a novel synthetic route for the preparation of well-defined and faceted nanocrystals of ternary rare earth oxychlorides based on the ligand exchange and condensation of rare earth halides and alkoxides in the presence of coordinating solvents. Nanocubes, faceted 2D nanosheets, and nanodisk morphologies are obtained as a result of preferential growth along specific crystallographic directions dictated by the choice of the rare earth ion and the capping ligand. The synthetic approach reported here represents a unique low-temperature route for the preparation of LnOCl in the PbFCl matlockite phase. The synthetic strategy can further be adapted to incorporate dopant ions. The potential applicability of these nanostructures as phosphors is illustrated by demonstrating the upconversion of near-infrared illumination to green and red emission by Er^{3+}:GdOCl nanocrystals.

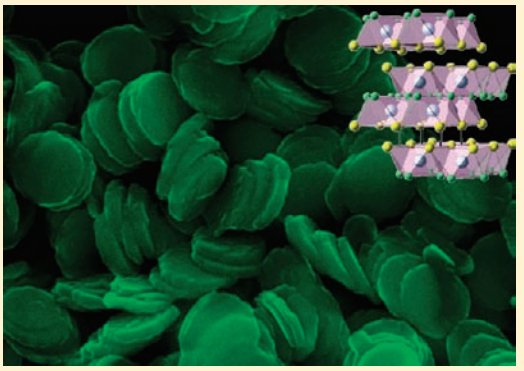

INTRODUCTION

The hot colloidal syntheses of ligand-capped inorganic nanocrystals from metal—organic precursors (either added directly or generated in situ) in high-boiling-point solvents has emerged as a mainstay and indeed a primary enabling tool for the discipline of nanoscience owing to the distinctive advantages bestowed upon materials prepared through these routes including unparalleled extent of surface passivation, high crystalline quality, monodispersity of particle dimensions and morphology, and the solution processability imparted by surface-capping ligands.[1−13] While the syntheses of metal, metal alloy, and binary chalcogenide nanocrystals are relatively mature at this point, truly ternary systems remain relatively underexplored. We present here a novel nonhydrolytic approach for the synthesis of well-defined faceted LnOCl (Ln = La, Ce, Gd, Dy, Er, Yb) nanocrystals based on the condensation of a rare earth metal halide with the apposite alkoxide. The synthetic chemistry reported here is hitherto unprecedented even in the bulk for the synthesis of rare earth oxyhalides.

Lanthanide oxychlorides represent an intriguing target for the exploration of finite size effects given their low maximum phonon cutoff energy, high chemical stability, and ability to promote efficacious phonon energy transfer to dopant ions, which have inspired extensive investigations for applications in optically stimulated and field-emission driven phosphors, X-ray detectors, upconversion lasers, and optical telecommunications infrastructure.[14−18] Rare earth oxyhalides are also rated as preeminent solid electrolytes, yielding the highest reported ion conductivities thus far for Cl^- and Br^- conduction, and have further proven to be remarkably robust heterogeneous catalysts for the chlorination of methane to methyl chloride as well as for the dechlorination of CCl_4 to more innocuous CO_2.[19−22] Obtaining nanocrystalline LnOCl with well-defined surface termination and dispersibility thus represents a worthwhile endeavor to facilitate fundamental investigations of finite size effects on the luminescence intensities and lifetimes of doped rare earth ions, conductivities for ionic and electronic carrier transport, and catalytic activity.

Some synthetic approaches reported thus far for the preparation of LnOCl nanocrystals include surfactant-mediated hydrothermal syntheses, mechanochemical grinding, sol—gel processes, and the modified pyrohydrolyisis of ternary ammonium chlorometalates.[17,18,23,24] While these synthetic routes are indeed successful in the fabrication of lanthanide oxychlorides with nanometer-scale dimensions, they induce scarcely little selectivity with regard to size, morphology, or crystallographic growth directions, and the prepared materials are best described as polydisperse nanopowders. To the best of our knowledge, only a single report has appeared thus far for the hot colloidal synthesis of LnOCl nanocrystals by controlled thermolysis of metal—organic precursors followed by nucleation and growth steps. Du et al. have used the thermolysis of lanthanum chloroacetate precursors in coordinating solvents for the preparation of ligand-capped LnOCl nanoplates based on modification of a methodology originally developed for the fabrication of LnF_3 and cubic LnOF nanocrystals.[25−27] We unveil a novel synthetic route based on the condensation of rare earth halides and alkoxides in the presence of coordinating ligands, trioctylphosphine oxide (TOPO) and oleylamine, which enables selective growth of nanocubes, nanodiscs, faceted nanosheets, and quasi-spherical

Received: January 18, 2011
Published: May 13, 2011

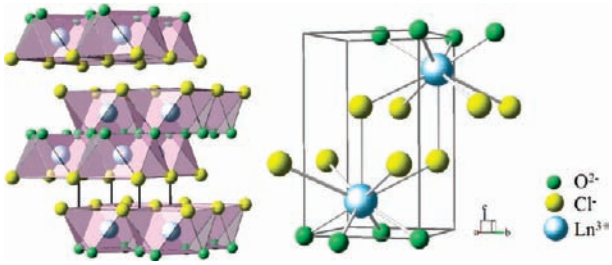

Figure 1. (A) The matlockite tetragonal PbFCl-type structure and (B) the local coordination environment of Ln-ions indicating a monocapped square antiprism local geometry.

nanoparticulate morphologies depending on the nature of the rare earth ion and the coordinating ligand and their specific interactions.

The lighter oxychlorides of the lanthanides crystallize in the matlockite tetragonal PbFCl structure (space group: *P4/nmm*; $Z = 2$) depicted in Figure 1a with alternating cationic layers of $(LnO)_n^{n+}$ and anionic layers of Cl^- arrayed along the crystallographic *c* direction. The local coordination environment of Ln is characterized by C_{4v} symmetry with the metal atom residing within a monocapped square antiprism, where it is surrounded by four oxygen atoms and five chlorine atoms, as depicted in Figure 1b. Notably, the fifth chloride ligand is distinctive from the remaining four proximal chlorides in being located in the next-to-nearest anionic layer.[28,29] Our synthetic approach has been optimized for the preparation of shape-controlled PbFCl nanocrystals of lanthanide oxychlorides but also yields nanocrystals for heavier lanthanides (Er and beyond), which tend to crystallize in a mixture of layered YOF and SmSI structures (Figure S1, Supporting Information, SI).[29−31] These structures are based on hexagonally packed bilayers of the heavier lanthanides sandwiched between hexagonally packed chloride layers with oxygen atoms residing in tetrahedral holes of the lanthanide layers.[31]

EXPERIMENTAL SECTION

Synthesis. $LaCl_3$, $CeCl_3$, $GdCl_3$, $DyCl_3$, $ErCl_3$, $YbCl_3$, $Ce(O^iPr)_4$, $Gd(O^iPr)_3$, $Dy(O^iPr)_3$, $Er(O^iPr)_3$, $Yb(O^iPr)_3$, and TOPO were purchased from Strem and used as received. $La(O^iPr)_3$ was purchased from Gelest, and oleylamine was purchased from Aldrich and used as received. In a typical synthesis, 2 mmol of anhydrous $LnCl_3$ and 2 mmol of $Ln(O^iPr)_3$ are weighed into a three-neck flask within an Ar-filled glovebox along with 25 mmol of the coordinating solvent (either TOPO or oleylamine). Subsequently, the reaction mixture is heated with stirring to 340°C under an argon atmosphere using standard Schlenk conditions. After heating for 2 h, the reaction mixture is allowed to cool to ~60°C and acetone or hexane is added depending on the coordinating ligand (TOPO and oleylamine, respectively) to flocculate the prepared nanocrystals. The nanocrystals are subsequently recovered by centrifugation at 12 000 rpm for 25 min with subsequent dispersion into hexane. A second washing/centrifugation is performed at 1500 rpm for 5 min to remove unreacted large particulates. Subsequently, the decanted dispersion of the nanoparticles is resuspended in hexane and centrifuged at 12 000 rpm to collect the nanocrystals (pelletized at the bottom of the centrifuge tube).

Characterization. The phase purity and composition of the products was examined by using X-ray diffraction (XRD) on a Rigaku Ultima IV diffractometer with Cu Kα radiation ($\lambda = 1.5418$ Å). The dimensions, morphology, and crystallinity of the as-synthesized nanostructures were examined by means of scanning electron microscopy (SEM) using a Hitachi SU-70 scanning electron microscope operated at an accelerating voltage of 20 kV and by transmission electron microscopy using a JEOL 2010 instrument operated at an accelerating voltage of 200 kV. To prepare the samples for HRTEM and selected area electron diffraction (SAED) analysis, the nanostructures were dispersed in 2-propanol and then deposited onto 300-mesh carbon-coated Cu grids. Raman measurements of powder samples were performed using a Horiba Jobin-Yvon LabRamHR single spectrometer instrument with an edge filter for rejection of the Rayleigh line and a Peltier-cooled CCD camera from Andor. Raman spectra for the nanocrystals were acquired using 784.5 nm laser excitation from a diode laser. Emission spectra were acquired using a Fluorolog-3.11 Horiba Jobin-Yvon spectrofluorometer under excitation at 376 and 980 nm for Tb^{3+} and Er^{3+}-doped GdOCl nanocrystals, respectively. The extent of doping in the nanocrystals was determined by inductively coupled plasma—mass spectrometry (ICP—MS) experiments performed on powder samples after acid digestion in 2% HNO_3 solution.

RESULTS AND DISCUSSION

In previous work, the nonhydrolytic sol—gel condensation of transition metal halides with metal alkoxides in coordinating solvents as per:

$$\equiv M-X + \equiv M—O—R \rightarrow \equiv M—O—M \equiv + R—X \quad (1)$$

has been established as an efficacious route for the largescale monodisperse fabrication of ligand-passivated metal oxide nanocrystals.[32−37] Nanocrystals of early transition metal oxides including solid-solution mixed metal oxides $Hf_xZr_{1-x}O_2$ with precisely tunable stoichiometry have been prepared by us and other researchers by a modification of this approach as per:

$$mMX_n + nM'(OR)_m \rightarrow M_mM'_nO_{nm} + nmRX \quad (2)$$

[34−37] Interestingly, for the lanthanides, a ligand exchange reaction seems to predominate instead of the equations depicted in 1 and 2 yielding rare earth chloroalkoxides as per:

$$MCl_n + M'(OR)_n \rightarrow MCl_{n-x}(OR)_x + M'Cl_x(OR)_{n-x} \quad (3)$$

[37] which initiates the formation of LnOCl nanocrystals by elimination of alkyl halides and/or dialkyl ethers as per

$$2LnCl_3 + Ln(O—{}^iPr)_3 \rightarrow 3LnOCl + 3{}^iPr—Cl \quad (4)$$

and

$$LnCl_3 + 2Ln(O—{}^iPr)_3 \rightarrow 3LnOCl + 3{}^iPr—O—{}^iPr \quad (5)$$

For example, the condensation of a ligand-exchanged dichloroalkoxide $LnCl_2(O^iPr)$ with the condensed moiety $(O^iPr)(Cl)—Ln—O—Ln(Cl)(O^iPr)$ yields the LnOCl framework with elimination of ^iPrCl.

Figure 2A,C shows LaOCl nanocrystals prepared via the condensation of lanthanum chloroalkoxides in the presence of oleylamine as the coordinating solvent. The nanocrystals have a distinctive cubic appearance with an edge size distribution centered at ~13.2 nm. Figure 3A illustrates the X-ray diffraction patterns that can be indexed to the matlockite PbFCl structure depicted in Figure 1 (Joint Committee on Powder Diffraction Standards (JCPDS) # 08−0477). Notably, the peak ascribed to reflections from (111) planes is unusually intense. The HRTEM image in Figure 2C indicates that the obtained nanocubes are single crystalline and indicates interplanar separation of the

dx.doi.org/10.1021/ic200114s |*Inorg. Chem.* 2011, 50, 5539–5544

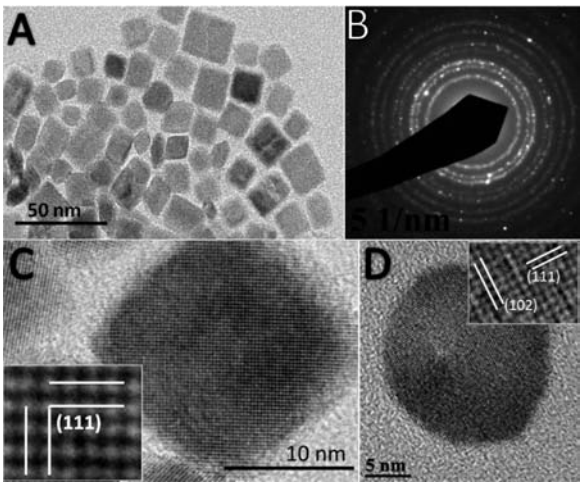

Figure 2. (A) TEM image of LaOCl nanocrystals formed using oleylamine as the coordinating solvent; (B) SAED pattern of LaOCl nanocrystals formed in oleylamine; and (C) lattice-resolved HRTEM image of an individual LaOCl nanocrystal. (D) Lattice-resolved image of an individual LaOCl nanocrystal synthesized using TOPO as the coordinating solvent.

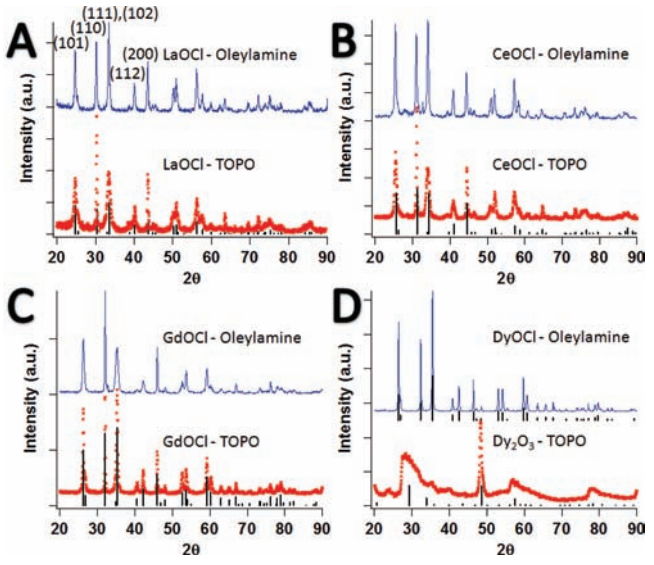

Figure 3. Powder X-ray diffraction patterns acquired for (A) LaOCl, (B) CeOCl, (C) GdOCl, and (D) DyOCl/Dy_2O_3 nanocrystals. In each panel, the top solid line depicts the diffraction pattern measured for nanocrystals prepared using oleylamine as the coordinating solvent, whereas the lower dotted line correponds to nanocrystals prepared using TOPO as the coordinating solvent. The intensities from the appropriate JCPDS files are also plotted in each case.

(111) planes. The growth of nanocubes and the ⟨111⟩ growth observed here is very distinctive from the confined ⟨110⟩ growth noted by Du et al. for LaOCl nanocrystals grown from a lanthanum tricholoroacetate precursor.[25] Notably, the use of TOPO induces a very different morphology that is more quasi-spherical in nature (Figure 2D). Further structural characterization of the prepared nanocrystals is derived from Raman spectroscopy experiments (Figure 4). All six Raman bands predicted by symmetry for the tetragonal PbFCl phase of LaOCl are clearly discernible in the Raman spectrum and are assigned

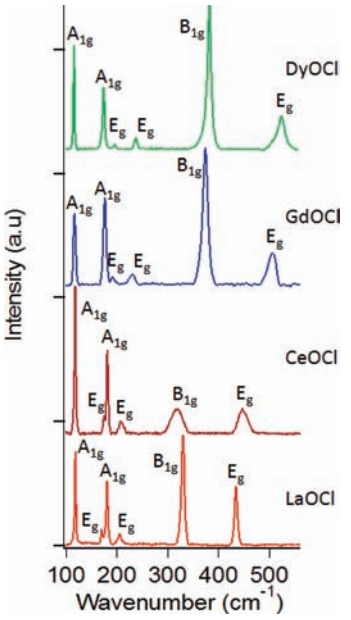

Figure 4. Raman spectra of LaOCl, CeOCl, GdOCl, and DyOCl nanocrystals prepared using oleylamine as the coordinating solvent.

to phonons with A_{1g}, E_g, and B_{1g} symmetries, as indicated in Figure 4.[21,38,39] The low-energy bands in the 175—210 cm^{-1} region predominantly involve phonon modes centered on La−Cl bond, whereas the bands >330 cm^{-1} in energy involve the motion of the oxygen atoms.[21]

In addition to the synthetic approach described here wherein the alkoxide and halide precursors are heated together in the coordinating solvent, we have also attempted a hot injection approach involving heating the lanthanum halide precursor to 340 °C and injecting the lanthanum alkoxide precursor that has separately been heated to the same temperature (or vice versa). Figure S2 (SI) shows XRD patterns and TEM images of the obtained products. The tetragonal matlockite phase is clearly obtained but there is no discernible improvement in monodispersity as is observed often with hot injection methods. We postulate that the need for ligand exchange (eq 3) to precede condensation (eqs 4 and 5) may give rise to the circumstance of better size and shape control being achieved upon jointly heating both reactants within the same mixture.

CeOCl nanocrystals have also been prepared via the condensation of cerium isopropoxide and cerium chloride. Rectangular nanosheet morphologies are obtained for CeOCl with 2D growth along the ⟨110⟩ direction in oleylamine and quasi-spherical platelets in TOPO (Figure 5). Figure 3B shows the XRD patterns for the CeOCl nanocrystals prepared using oleylamine and TOPO as coordinating solvents.

Figure 3C shows powder XRD patterns for GdOCl nanocrystals synthesized by the condensation reactions depicted in eqs 4 and 5 in the presence of oleylamine and TOPO as the coordinating solvents. Both XRD patterns can be indexed to the tetragonal PbFCl structure (JCPDS# 85−1199) but the relative intensities of the reflections show some interesting differences. The (110) peak is the narrowest and most prominent feature for GdOCl nanocrystals synthesized in the presence of oleylamine as the coordinating solvent, whereas the (102) reflection is the most pronounced feature for the nanocrystals synthesized in TOPO. The morphologies of the GdOCl nanocrystals are also very

dx.doi.org/10.1021/ic200114s |*Inorg. Chem.* 2011, 50, 5539–5544

different depending upon the coordinating solvent. Reaction in oleylamine yields ultrathin rectangular nanosheets with lateral dimensions of ~80 nm, as shown by the TEM images in Figure 6B and the SAED pattern acquired for the ensemble of particles in Figure 6C. In contrast, Figure 6D—F indicates the growth of single crystalline nanodisc structures when the reaction is performed using TOPO as the coordinating solvent.

The selective binding of ligand molecules to specific crystallographic facets leads to preferential crystalline growth by monomer addition onto the other more accessible facets, and has emerged as a vital albeit quasi-empirical means for controlling the shape of nanomaterials.[25,26,40−43] For example, Hyeon and co-workers were able to dramatically demonstrate the confinement of Sm_2O_3 nanoplatelets and nanowires to thicknesses that spanned only two unit cells in height.[43] The GdOCl nanosheets capped with oleylamine show a distinctive preference for 2D growth along the ⟨110⟩ directions indicating strong confinement along the crystallographic *c* axis due to coordination of oleylamine to Gd^{3+} ions along the ⟨001⟩ facets (akin to replacing the most distal Cl^- in the Gd^{3+} coordination sphere). Remarkably, in the presence of the less basic TOPO ligand, growth appears to be favored along the ⟨*h*0*l*⟩ direction as well, as suggested by the relatively greater thickness of the obtained stacked nanodisks. Figure 6D illustrates the relatively rough 2D cross-section although the obtained nanodisks appear to be fairly monodisperse in shape and size with lateral dimensions of ~395 ± 10 nm. The disks exhibit a tendency to stack face-to-face through interactions that may be mediated by the capping ligands.[25,26] Notably, in the use of TOPO as a ligand, adventitious impurities such as phosphonic acids with varying chain lengths have been implicated.[44,45] Selective binding of these ligands to different LnOCl facets may also engender some selectivity of growth direction. The preferential binding of ligand molecules with varying basicity to different crystallographic facets of incipient LnOCl nanocrystal nuclei thus enhances monomer addition and crystal growth along specific directions, greatly modifying the morphologies of the obtained products.

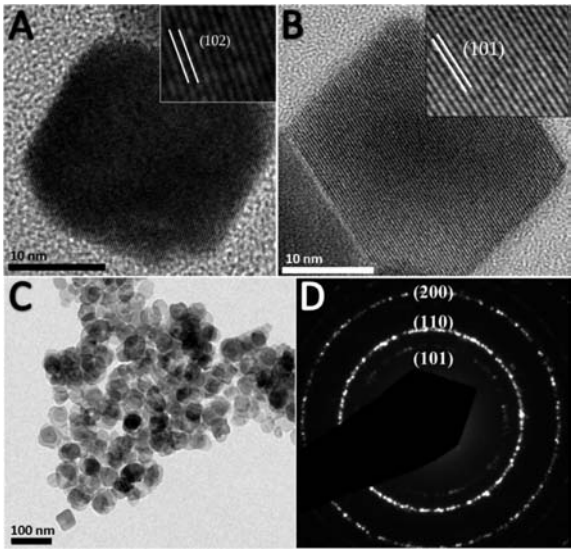

Figure 5. (A,B) TEM images of CeOCl nanocrystals formed using oleylamine as the coordinating solvent. The insets show lattice-resolved images. (C) TEM image of CeOCl nanocrystals synthesized using TOPO as the coordinating solvent. (D) SAED pattern of an ensemble of CeOCl nanocrystals synthesized using TOPO as the coordinating solvent.

Notably, the metal isopropoxide moieties could also show distinctive hydrogen-bonding behavior in TOPO and oleylamine, which could alter the kinetics of growth along different crystallographic facets giving rise to the differences in the obtained morphologies.

Remarkably, the distinctive Lewis base/hydrogen-bonding characters of the two ligands are manifested in a more pronounced manner as we go across the lanthanide series. Figure 7A, B indicate the stabilization of single-crystalline DyOCl nanosheets with regular octagonal cross sections and lengths centered around 970 nm again suggestive of 2D growth when the condensation reaction is performed in oleylamine. The octagonal sheets exhibit a pronounced tendency to stack in a face-to-face manner as depicted in the inset to Figure 7B. The XRD pattern of the prepared nanocrystals can be indexed to JCPDS # 47−1725 (Figure 3D), again suggesting the stabilization of the tetragonal PbFCl phase. However, when the reaction is performed in TOPO, the oxychloride is no longer stabilized and instead quasi-spherical nanoparticles of the oxide phase Dy_2O_3 are obtained likely due to preferential alkyl halide

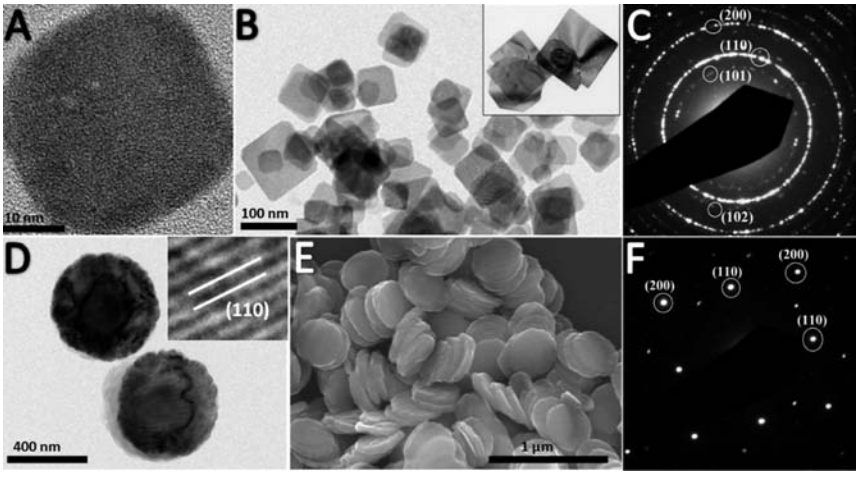

Figure 6. (A) and (B) TEM images of GdOCl nanosheets formed using oleylamine as the coordinating solvent; the inset shows individual nanosheets with square cross sections. (C) SAED pattern of GdOCl nanocrystals formed in oleylamine. (D) TEM, (E) SEM, and (F) SAED pattern of GdOCl nanocrystal formed in TOPO. The inset to (D) depicts a high-resolution TEM image of an individual GdOCl nanocrystal.

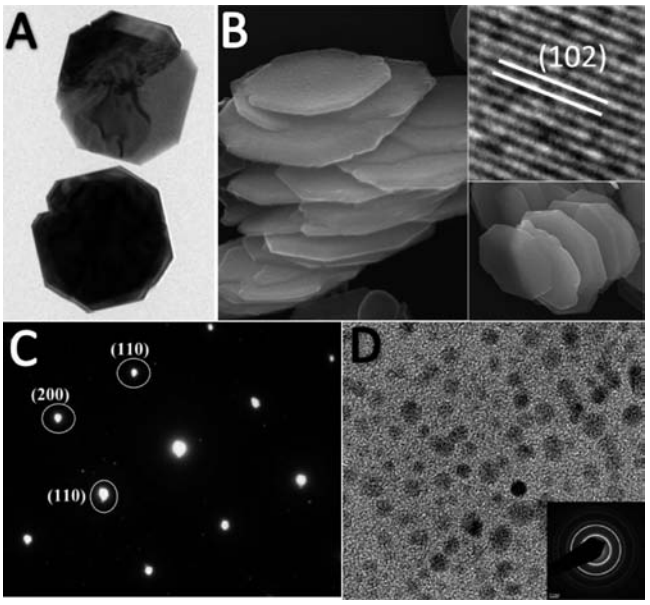

Figure 7. (A) TEM, and (B) SEM images of DyOCl nanocrystals prepared in oleylamine; the lower inset illustrates the face-to-face stacking of the platelets, whereas the top inset illustrates a lattice-resolved TEM image of a single DyOCl nanocrystal. (C) SAED pattern acquired for a single DyOCl nanosheet prepared in oleylamine. (D) TEM image of Dy_2O_3 nanocrystals synthesized using TOPO as the coordinating solvent with the corresponding SAED pattern shown as an inset.

elimination as per eq 1. The nanoparticles are also significantly different in size, <10 nm in diameter (Figure 7D), further suggesting the operation of an entirely different mechanistic pathway. Notably, dysprosium is significantly more acidic than lanthanum due to poor shielding by the *f* electrons, and the competing kinetics of the condensation versus ligand exchange reactions are likely to depend greatly on the Lewis base strengths of the ligands. We have previously evidenced the sensitivity of the kinetics of the two competing reactions (influencing the composition of the final product) not by changing the ligand but by altering the alkoxide precursor; condensation of cerium halides with $Ce(O—^{i}Pr)_4$ yields CeOCl nanocrystals as per eqs 4 and 5, whereas reaction with $Ce(O—^{tert}but)_4$ yields $CeO_{2-\delta}$ nanocrystals as per eq 1.[37] Analogously, Du et al. have also found that the addition of oleic acid to their reactions involving the thermolysis of $La(CCl_3COO)_3$ in oleylamine promotes the stabilization of La_2O_3 nanocrystals.[25]

The Raman spectra for the CeOCl, GdOCl, and DyOCl nanocrystals further corroborate the phase identification (Figure 4). A pronounced shift to higher frequencies is noted particularly for the relatively higher energy B_{1g} and E_g modes, reflecting the stronger Ln—O bonding due to increased Lewis acidity of the metal sites (as well as the increase in atomic weight).

Proceeding further along the lanthanide series, analogous reactions have been attempted for erbium and ytterbium. A similar preference for stabilization of the oxychloride in oleylamine but the sesquioxide in TOPO is observed for both the heavier lanthanides (Figures S3 and S4, SI). Notably, however, as is characteristic of the heavier lanthanides, the oxychlorides are no longer in the tetragonal PbFCl structure but instead crystallize as a mixture of YOF and SmSI phases. Considerably, greater agglomeration and a less regular hexagonal shape is noted for these nanoplatelets suggesting that oleylamine is not ideal for

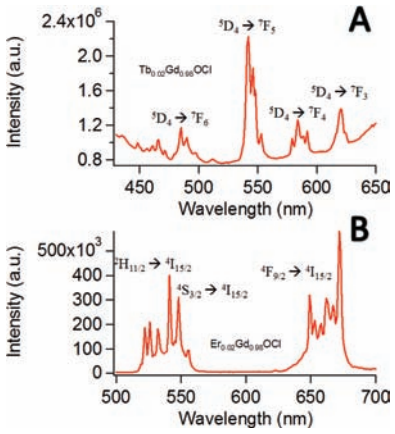

Figure 8. Emission spectra of (A) $Tb_{0.02}Gd_{0.98}OCl$ acquired at an excitation of 376 nm and (B) $Er_{0.02}Gd_{0.98}$ OCl acquired at 980 nm excitation.

binding to the exposed crystallographic facets of the layered YOF and SmSI phases. Optimization of nanocrystalline growth for heavier lanthanides with their distinctive crystal structures will be the subject of future work and will require the identification of suitable ligands.

For the PbFCl matockite phase, we have performed a preliminary investigation of the applicability of our synthetic approach to the preparation of solid-solution nanocrystals with doped rare-earth ions, such as will be required for the fabrication of phosphors.[16,18,23,28] Specifically, Tb^{3+} and Er^{3+} ions were substitutionally doped into GdOCl by replacing the appropriate molar equivalent of $GdCl_3$ in the synthetic scheme with $TbCl_3$ or $ErCl_3$. Figure 8 shows emission spectra acquired at 376 and 980 nm excitation for $Tb_{0.02}Gd_{0.98}OCl$ and $Er_{0.02}Gd_{0.98}OCl$ nanocrystals, respectively, wherein the stoichiometries have been verified by ICP-MS experiments. The low dopant concentrations have been selected to exclude self-quenching effects.[28]

Figure 8a shows strong green emission originating from $^5D_4 \rightarrow {}^7F_J$ ($J = 6—3$) relaxations of the Tb^{3+} ion doped within the GdOCl lattice.[27] The observed fine structure originates from the crystal field effects due to the reduced C_{4v} symmetry of the substitutionally doped Tb^{3+} ion (as compared to the completely symmetric free ion). Figure 8b clearly shows the upconversion of 980 nm laser illumination to finely structured green emission in the 515—550 nm range and equally well structured red emission in the 650—670 nm range for $Er_{0.02}Gd_{0.98}OCl$ solid-solution nanocrystals. The green bands centered at 526 and 545 nm can be attributed to $^2H_{11/2} \rightarrow {}^4I_{15/2}$ and $^4S_{3/2} \rightarrow {}^4I_{15/2}$ transitions of the dopant Er^{3+} ions.[15,17,27] The higher energy states are thought to be populated by two-photon-induced excited state absorption and cross relaxation processes.[17,27] The red emission centered at ~670 nm can be ascribed to the $^4F_{9/2} \rightarrow {}^4I_{15/2}$ relaxation from an excited state thought to be populated by phonon energy transfer processes from an adjacent Er^{3+} ion that is present in an excited state (with a long lifetime) transmitted via the GdOCl host lattice.[17] The limited set of data presented here suggests that the developed synthetic route is amenable to the incorporation of substitutional dopants that preserve their distinctive luminescence properties including upconversion of near-infrared illumination to visible emission.

In closing, we report a novel synthetic strategy for the preparation of well-defined rare earth oxychloride nanostructures with

dx.doi.org/10.1021/ic200114s |*Inorg. Chem.* 2011, 50, 5539–5544

regular shapes based on the ligand exchange and condensation of rare earth chlorides and rare earth alkoxides in the presence of a coordinating solvent. The selective adsorption of the coordinating solvent (TOPO or oleylamine) to specific crystallographic facets of the incipient LnOCl nuclei determines the growth direction and thus the final morphology of the obtained product. This enables the stabilization of a wide diversity of shapes ranging from nanocubes to octagonal and rectangular nanosheets and nanodiscs. The prepared methodology yields regularly shaped nanocrystals of the PbFCl structure type for early lanthanides and less regular but still nanocrystalline powders of mixed YOF and SmSI phases for heavier lanthanides. Additionally, the synthetic approach permits the incorporation of substituitional rare earth dopants, and upconversion has been demonstrated for an Er^{3+}:GdOCl system with potential relevance for photovoltaic coatings and two-photon imaging. Future work will focus on stabilization of heavier lanthanides and exploration of intercalative properties at the nanoscale. The design of suitable ligands tailored for high affinity to lanthanides will also be explored to expand the repertoire of available nanocrystal morphologies.

■ ASSOCIATED CONTENT

Supporting Information. TEM images and XRD patterns of ErOCl and YbOCl nanocrystals. Characterization data for LaOCl nanocrystals prepared by the hot injection method. Depiction of hexagonal SmSI-type structure adopted by heavier lanthanide oxychlorides. Figures S1−S3. This material is available free of charge via the Internet at http://pubs.acs.org.

■ AUTHOR INFORMATION

Corresponding Author
*E-mail: sb244@buffalo.edu.

■ ACKNOWLEDGMENT

This work was primarily supported by the National Science Foundation under DMR 0847169. Partial support of this work through a Doctoral New Investigator Award from the American Chemical Society is also acknowledged. We are also grateful to the Research Corporation for Science Advancement for support through a Cottrell Scholar Award. Also, we would like to express our gratitude towards Dr. Paras Prasad for the use of his fluorimeter and Dr. Guanying Chen for his help with acquiring the emission spectra.

■ REFERENCES

(1) Murray, C. B.; D.J, N.; Bawendi, M. B. *J. Am. Chem. Soc.* **1993**, *115*, 8706.
(2) Murray, C. B.; Kagan, C. R.; Bawendi, M. G. *Annu. Rev. Mater. Sci.* **2000**, *30*, 546.
(3) Manna, L.; Scher, E. C.; Alivisatos, A. P. *J. Am. Chem. Soc.* **2000**, *122*, 12700.
(4) Peng, Z. A.; Peng, X. *J. Am. Chem. Soc.* **2002**, *124*, 3343.
(5) Peng, X. *Adv. Mater.* **2003**, *15*, 459.
(6) Talapin, D. V.; Nelson, J. H.; Shevchenko, E. V.; Aloni, S.; Sadtler, B.; Alivisatos, A. P. *J. Am. Chem. Soc.* **2007**, *129*, 11354.
(7) Rogach, A. L.; Talapin, D. V.; Shevchenko, E. V.; Kornowski, A.; Haase, M. A.; Weller, H. *Adv. Funct. Mater.* **2002**, *12*, 653.
(8) Senevirathne, K.; Tackett, R.; Kharel, P. R.; Lawes, G.; Somaskandan, K.; Brock, S. L. *ACS Nano* **2009**, *3*, 1129.
(9) Yu, H.; Liu, Y.; Brock, S. L. *Inorg. Chem.* **2008**, *47*, 1428.
(10) Yin, M.; O'Brien, S. *J. Am. Chem. Soc.* **2003**, *125*, 10180.
(11) Luo, J.; Han, L.; Kariuki, N.; Wang, L.; Mott, D.; Zhong, C. J.; He, T. *Chem. Mater.* **2005**, *17*, 5282.
(12) Maye, M. M.; Zheng, W. X.; Leibowitz, F. L.; Ly, N. K.; Zhong, C. J. *Langmuir* **2000**, 16.
(13) Liu, H. T.; Owen, J. S.; Alivisatos, A. P. *J. Am. Chem. Soc.* **2007**, *129*, 305.
(14) Van Uitert, L. G.; Levinstein, H. J.; Grodkiewiecz, W. H. *Mater. Res. Bull.* **1969**, *4*, 381.
(15) Rambabu, U.; Annapurna, K.; Balaji, T.; Buddhudu, S. *Mater. Lett.* **1995**, *23*, 143.
(16) Holsa, J.; Lamminmaki, R.-J.; Latusaari, M.; Porcher, P. *J. Alloys Compd.* **2001**, *323*−*324*, 811.
(17) Konishi, T.; Shimizu, M.; Kameyama, Y.; Soga, K. *J. Mater. Sci. Mater. Electron.* **2007**, *18*, S183.
(18) Li, G.; Li, C.; Zhang, C.; Cheng, Z.; Quan, Z.; Peng, C.; Lin, J. *J. Mater. Chem.* **2009**, *19*, 8936.
(19) Imanaka, N.; Okamoto, K.; Adachi, G.-Y. *Angew. Chem., Int. Ed.* **2002**, *41*, 3890.
(20) Imanaka, N.; Kato, Y. *Chem. Commun.* **2003**, 1270.
(21) Podkolzin, S. G.; Strangland, E. E.; Jones, M. E.; Peringer, E.; Lercher, J. A. *J. Am. Chem. Soc.* **2005**, *129*, 2569.
(22) Van der Avert, P.; Weckhuysen, B. M. *Angew. Chem., Int. Ed.* **2002**, *41*, 4730.
(23) Lee, S.-S.; Park, H.-I.; Joh, C.-H.; Byeon, S.-H. *J. Solid State Chem.* **2007**, *180*, 3529.
(24) Lee, J.; Zhang, Q.; Saito, F. *J. Solid State Chem.* **2001**, *160*, 469.
(25) Du, Y.-P.; Zhang, Y.-W.; Sun, L.-D.; Yan, C.-H. *J. Am. Chem. Soc.* **2009**, *131*, 3162.
(26) Sun, X.; Zhang, Y.-W.; Du, Y.-P.; Yan, Z.-G.; Si, R.; You, L.-P.; Yan, C.-H. *Chem.—Eur. J.* **2007**, *13*, 2320.
(27) Du, Y.-P.; Zhang, Y.-W.; Sun, L.-D.; Yan, C.-H. *J. Phys. Chem. C* **2008**, *112*, 405.
(28) Holsa, J.; Sailynoja, E.; Lamminmaki, R.-J.; Deren, P.; Strek, W.; Porcher, P. *J. Chem. Soc. Faraday Trans.* **1997**, *93*, 2241.
(29) Garcia, E.; Corbett, J. D.; Ford, J. E.; Vary, W. J. *Inorg. Chem.* **1985**, *24*, 494.
(30) Odink, D. A.; Song, K.; Kauzlarich, S. M. *Chem. Mater.* **1992**, *4*, 906.
(31) Song, K.; Kauzlarich, S. M. *J. Alloys Compd.* **1994**, *207/208*, 427.
(32) Trentler, T. J.; Denler, T. E.; Bertone, J. F.; Agrawal, A.; Colvin, V. L. *J. Am. Chem. Soc.* **1999**, *121*, 1613.
(33) Joo, J.; Yu, T.; Woon Kim, Y.; Min Park, H.; Wu, F.; Zhang, J. Z.; Hyeon, T. *J. Am. Chem. Soc.* **2003**, *125*, 6553.
(34) Tang, J.; Fabbri, J.; Robinson, R. D.; Zhu, Y.; Herman, I. P.; Steigerwald, M. L.; Brus, L. E. *Chem. Mater.* **2004**, *16*, 1336.
(35) Tang, J.; Zhang, F.; Zoogman, P.; Fabbri, J.; Chan, S.-W.; Zhu, Y.; Brus, L. E.; Steigerwald, M. S. *Adv. Funct. Mater.* **2005**, *15*, 1595.
(36) Depner, S. W.; Kort, K. R.; Banerjee, S. *CrystEngComm* **2009**, *11*, 841.
(37) Depner, S. W.; Kort, K. R.; Jaye, C.; Fischer, D. A.; Banerjee, S. *J. Phys. Chem. C* **2009**, *113*, 14126.
(38) Holsa, J.; Kestila, E.; Koski, K.; Rahiala, H. *J. Alloys Compd.* **1995**, *225*, 193.
(39) Weckhuysen, B. M.; Rosynek, M. P.; Lunsford, J. H. *Phys. Chem. Chem. Phys.* **1999**, *1*, 3157.
(40) Puzder, A.; Williamson, A. J.; Zaitseva, N.; Manna, G. G.; Alivisatos, A. P. *Nano Lett.* **2004**, *4*, 2361.
(41) Puntes, V. F.; Zanchet, D.; Erdonmez, C. K.; Alivisatos, A. P. *J. Am. Chem. Soc.* **2002**, *124*, 12874.
(42) Sigman, M. B., Jr.; Ghezelbash, A.; Hanrath, T.; Saunders, A. E.; Lee, F.; Korgek, B. A. *J. Am. Chem. Soc.* **2003**, *125*, 16050.
(43) Yu, T.; Joo, J.; Park, Y. I.; Hyeon, T. *J. Am. Chem. Soc.* **2006**, *128*, 1786.
(44) Wang, F.; Tang, R.; Buhro, W. E. *Nano Lett.* **2008**, *8*, 3521.
(45) Wang, F.; Tang, R.; Kao, J. L.-F.; Dingman, S. D.; Buhro, W. E. *J. Am. Chem. Soc.* **2009**, *131*, 4983.